

Hydrogen Production and Heat Transfer Distributions of Ammonia Decomposition in an Atmospheric Pressure Plasma Plate Reactor

Mostafa El-Shafie^{*1}, Shinji Kambara², Yukio Hayakawa³

¹Environmental and Renewable Energy Systems Division, Graduate School of Engineering, Gifu University, 1-1 Yanagido, Gifu, 501-1193, Japan

e-mail: mostafaelshafie81@gmail.com

²Environmental and Renewable Energy Systems Division, Graduate School of Engineering, Gifu University, 1-1 Yanagido, Gifu, 501-1193, Japan

e-mail: kambara_obsolete@gifu-u.ac.jp

³Environmental and Renewable Energy Systems Division, Graduate School of Engineering, Gifu University, 1-1 Yanagido, Gifu, 501-1193, Japan

e-mail: h_yukio@gifu-u.ac.jp

Cite as: El-Shafie, M., Kambara, S., Hayakawa, Y., Hydrogen Production and Heat Transfer Distributions of Ammonia Decomposition in an Atmospheric Pressure Plasma Plate Reactor, J. sustain. dev. energy water environ. syst., 1080347, DOI: <https://doi.org/10.13044/j.sdewes.d8.0347>

ABSTRACT

This study extensively investigated the hydrogen production and heat transfer distribution in atmospheric pressure dielectric barrier discharge plasma reactor. Ammonia gas was fed into a plasma plate reactor at flow rates of 0.1-1 L/min with different electrode gap distances of 1 mm and 4.5 mm. The heat transfer distribution was determined for the metallic and dielectric electrodes. The maximum conversion rates of the reactor with electrode gap distances of 4.5 mm, 1 mm were 83% and 19.2%, respectively. At a reactor electrode gap distance of 4.5 mm, the maximum energy efficiencies were 0.193%, 0.178%, and 0.105% at ammonia input flow rates of 1, 0.5, and 0.1 L/min, respectively. The results at an electrode gap distance of 1 mm were 0.042%, 0.038%, and 0.022% at ammonia input flow rates of 1, 0.5 and 0.1 L/min, respectively.

KEYWORDS

Heat transfer, Energy distribution, dielectric barrier discharge plasma, Hydrogen production.

INTRODUCTION

Ammonia gas is considered an important hydrogen energy carrier and can deliver CO_x-free hydrogen for different applications, such as fuel cells [1]. In recent decades, different studies have evaluated hydrogen storage [2]. Fossil fuels and renewable energy sources are the most used methods to produce hydrogen and include coal, natural gas, biomass, hydropower, geothermal, solar, and wind energy [3]. Methods of hydrogen production from fossil fuel and biomass resources have been extensively investigated, such as steam, partial oxidation, auto thermal, plasma, aqueous phase, and pyrolysis methods [4].

* Corresponding author

A number of renewable energy projects have applied a methodology to evaluate the effectiveness of instruments to increase energy efficiency to 45% by 2030 [5]. Most of the available hydrogen in the market is produced by steam reforming and water electrolysis. The energy balance of experimental and theoretical catalytic steam reforming reactions has been investigated [6]. Steam methane reforming has been performed over a mixed Ni/ MgAl and iron or chromium promoted M/Ni/MgAl catalysts [7]. Hydrogen production vapor has been investigated using Dielectric Barrier Discharge (DBD) plasma from different materials such as ammonia, hydrocarbons, water vapor, and biomass fuels.

A nonlinear autoregressive model was used to predict the syngas temperature and composition of biomass gasification during plant operation with different operating conditions [8]. Non-thermal plasma was used to assist the decomposition of benzene as a tar analogue [9]. Gliding arc non-thermal plasma has also been used to generate hydrogen (H_2) and hydrogen peroxide (H_2O_2) [10]. Preliminary results have been investigated for hydrogen production from water vapor [11]. A kinetic model has been provided for hydrogen production from water vapor plasmolysis at atmospheric pressure in a DBD micro-channel reactor [12].

Recently, the development of DBD plasma at atmospheric pressure has increased [13]. DBD plasma involves a specific type of alternating current (AC) discharge at atmospheric pressure.

It provides non-equilibrium plasma with good thermodynamics. DBD plasma is mostly effective in chemical and physical processes of gases [14]. The main advantages of DBD plasma are its ability to produce highly reactive plasma at room temperature with low electric power consumption and a short time response [15]. However, recent DBD plasma applications have had unfavorable temperature increases due to the use of modern reactors and operation at higher frequency.

DBD plasma has been applied in several applications, such as pollutant removal [16], biomedical applications [16], surface treatment [18], and flow control [19]. The heat generated by atmospheric-pressure or non-equilibrium DBD plasma often causes energy waste. Therefore, most of the plasma applications use an external cooling circuit. The resulting temperature rise from plasma is significantly affected by various chemical and electronic processes. To have better operating conditions, the plasma temperature must be controlled appropriately. Several attempts have been made to understand the heat transfer mechanism. Plasma diagnostics, computer modeling, and detailed experimental analyses have been developed to recognize local temperatures [20].

Atmospheric-pressure DBD plasma can be characterized as weakly ionized plasma with properties resembling transient high-pressure glow discharge properties. Due to the presence of a dielectric barrier material, the energy input into the plasma system is limited. However, the gas temperature of the DBD plasma in practical applications has increased, and the plasma reaction field strongly depends on the plasma properties and external cooling conditions.

Several studies on the heat transfer across plasma reactors have been developed [21]. The reactor heating temperature effect on the steam decomposition using DBD plasma has been investigated [22]. The heat transfer mechanism characteristics in methane-DBD plasma have been investigated [23]. A numerical simulation has been used to analyze the momentum and heat transfer of argon (Ar) gas in a needle-to-plane DBD reactor [24]. DBD plasma ignition obviously generates non-uniform Joule heating. Therefore, more information is needed about the heat transfer characteristics in atmospheric-pressure or DBD plasma to optimize them for plasmas applications.

The current study reports on the hydrogen production and heat transfer distribution across a plasma Plate Type Reactor (PPR) using 0.5% ammonia-argon as a base gas. The effects of the electrode gap distance and residence time on the ammonia decomposition were investigated. The heat transfer distributions across the PPR were analyzed at different voltages, and the total heat transfer rate and overall heat transfer coefficient were determined at different operating conditions. The energy efficiency results of reactor experiments were also compared.

EXPERIMENTAL

Ammonia-argon base gas with a concentration of 0.5% was decomposed into hydrogen and nitrogen gas by DBD in PPR at atmospheric pressure. **Figure 1** shows a diagram of the experimental setup. Ammonia gas was fed into the electrode gap distance of the PPR between both electrodes. Quartz glass was used as a dielectric with a thickness of 2 mm. A high-voltage electrode was connected to a copper mesh, which had a thickness of 0.25 mm. A metal plate (SUS 316) was used as the ground electrode and connected to an oscilloscope.

The plasma was generated using a power source with a 10-kHz sinusoidal voltage of 12-18 kV. The DBD plasma was produced with a discharge area of 45 mm × 45 mm. Measurements were taken for two different electrode gap distances of 4.5 mm and 1 mm. The decomposed gases were collected from the outlet reactor port using a syringe. The collected samples were analyzed using gas phase chromatography (GC, GC-2014S, SHIMADZU). The GC device was calibrated, and the error was estimated to be within ±5%. The input power was determined by a power meter, and the temperature was measured using K-type thermocouples connected at different PPR points. The feed gas was controlled by a Mass Flow Controller (MFC).

Figure 2 shows a photo of the PPR assembly photo without plasma and at plasma ignition. The gas inlet, outlet, and PPR surface temperatures were measured by K-type thermocouples. Ammonia gas was fed into the PPR discharge gap at 0.1-1 L/min at atmospheric pressure (100 kPa) and ambient temperature. The plasma discharge power was determined at different voltages using the power meter. The DBD plasma was generated in the discharge gap between the high-voltage electrode and the ground electrode. The energy distributions across the ground electrode, high-voltage electrode, and heat loss are discussed.

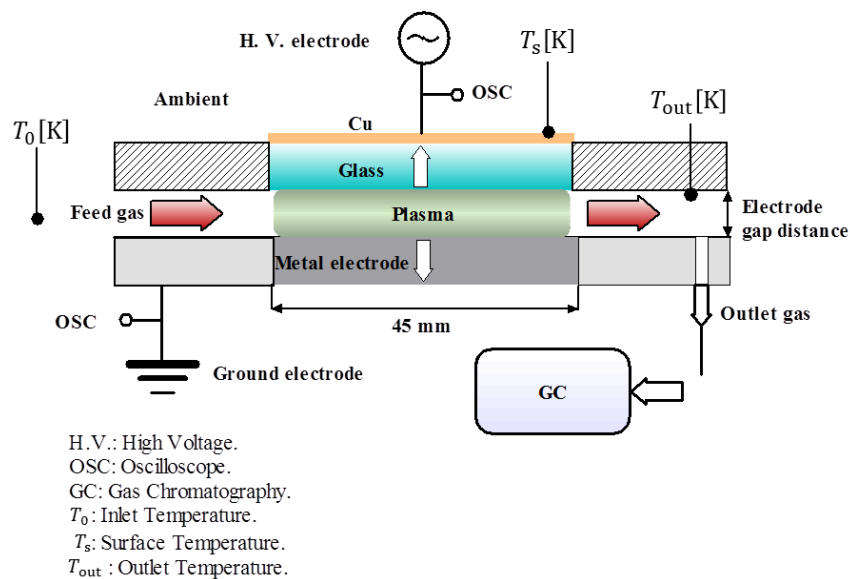


Figure 1. Experimental setup



Figure 2. Plasma plate reactor photos

Energy distribution

The energy equation for heat transfer by conduction of macroscopic expression is [21]:

$$\rho C_{p,g} u \frac{\partial T}{\partial x} = \lambda \left(\frac{\partial^2 T}{\partial x^2} + \frac{\partial^2 T}{\partial y^2} \right) + G \quad (1)$$

where x [m] is the gas flow direction, y [m] is the perpendicular direction to flow, G [Wm^{-3}] is the heat generation rate per unit volume, T [K] is the gas temperature, u [ms^{-1}] is the gas velocity, $\rho C_{p,g}$ [$\text{Jm}^{-3}\text{K}^{-1}$] is the heat capacity of the feeding ammonia gas, and λ [$\text{Wm}^{-1}\text{K}^{-1}$] is the thermal conductivity. The heat conduction equation has been used by many studies for modeling in DBD plasma analysis [19]. Uniform heat generation has been produced by micro discharges.

Figure 3 shows the heat transfer resistances across the reactor. This figure shows the heat flow from the plasma discharge gap to the high-voltage electrode. The total heat transfer rate can be determined with the following equation [25]:

$$dQ = U (T_g - T_a) dA \quad (2)$$

where U [$\text{W/m}^2\text{K}$] is the overall heat transfer coefficient, A [m^2] is the total heat transfer area, T_g and T_a [K] is the gas temperature and the PPR's surrounding temperature. The convection heat transfer from the inner plasma to the dielectric glass is obtained based on the gas input conditions. The conduction heat transfer resistances through the metal and dielectric electrodes are calculated according to eq. (1).

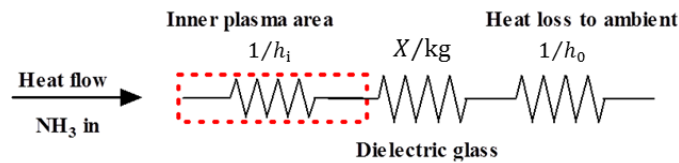


Figure 3. Heat transfer resistances from inner plasma to high-voltage electrode direction

The heat loss resistance from the high-voltage electrode surface to atmosphere was determined using Churchill and Chu's [26] Nusselt number relation:

$$\text{Nu} = 0.68 + \frac{0.670 \text{Ra}^{1/4}}{[1 + (0.492/\text{Pr})^{9/16}]^{4/9}} \quad (3)$$

where Pr is the Prandtl number, and Ra is the Rayleigh number ($\text{Ra} = \text{Gr} \times \text{Pr}$). The Grashof number was estimated from the following relation:

$$\text{Gr} = \frac{g\beta(T_s - T_a)L^3}{\nu^2} \quad (4)$$

where β [K^{-1}] is the thermal expansion coefficient, ν [m^2/s] is the kinematic viscosity, L [m] is the gap length, $g = 9,80665 \text{ m}^2/\text{s}$ as standard gravitational acceleration, and T_s and T_a [K] is the reactor-surface and ambient temperatures, respectively. The external heat transfer coefficient can be obtained from the Nusselt number relation ($\text{Nu} = h_o/k_{\text{airj}}$).

RESULTS AND DISCUSSION

Ammonia as an energy carrier contains more hydrogen than other liquids. Atmospheric-pressure plasma is characterized as weak plasma due to the limited energy fed into the plasma

system. The effects of the electrode gap distance at different ammonia (NH₃) flow rates were examined, and the heat transfer distribution was determined for both electrode gap distances.

Electrode gap distance effect

Figure 4 demonstrates the H₂ concentration obtained at different flow rates and electrode gap distances. The H₂ concentration at a gap distance of 4.5 mm was higher than that at 1 mm at all flow rates. The concentration of the H₂ also increased with the voltage. To clarify the effect of the gap distance, the produced H₂ flow rate was compared between ammonia gas flow rates of 0.1 and 1 L/min. The H₂ gas flow rate was determined based on GC concentration analysis. Figure 5 shows the results. The hydrogen flow rate at a gap distance of 4.5 mm was higher than that at 1 mm.

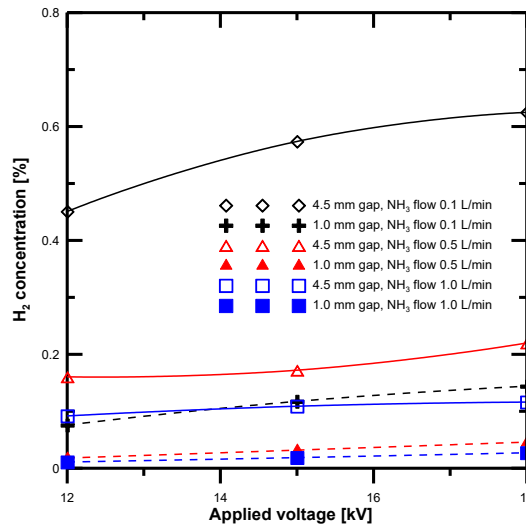


Figure 4. Comparison of hydrogen concentration at different discharge gap distances

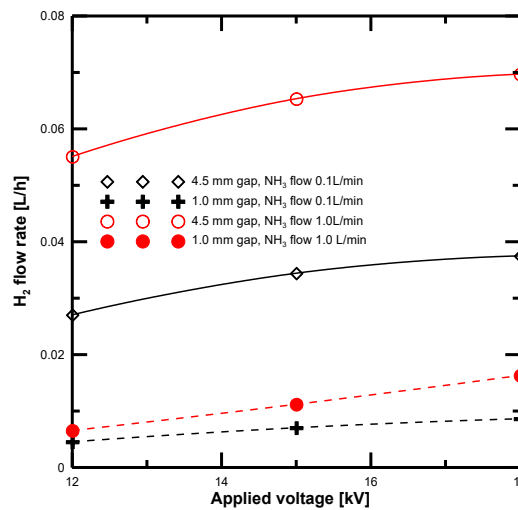


Figure 5. H₂ flow rate vs. voltage at different discharge gap distances

It was clear that the ammonia decomposition was improved with increasing gap distance. The residence time of ammonia decomposition can be determined based on the feed gas flow rate and the electrode gap distance. The ammonia conversion rate was calculated according to the following relation:

$$\text{NH}_3 \text{ conversion rate [\%]} = \text{H}_2 \text{ conc. [\%]} / ([\text{NH}_3]_0 \text{ conc.} \times 1.5) \times 100 \quad (5)$$

where H_2 conc is the produced hydrogen gas concentration at the PPR exit, and $[NH_3]_0$ is the initial ammonia concentration.

Figure 6 shows the conversion rate of ammonia at different plasma voltages and residence times with a gap distance of 4.5 mm. The conversion rate increased with the residence time and reached a maximum value of 83.65% at a voltage of 18 kV and NH_3 input flow rate of 0.1 L/min. Similarly, the conversion rate of ammonia decomposition with a gap distance of 1 mm is shown in **Figure 7**, where the conversion rate shows the same trend. The maximum rate was 19.28% at 18 kV and 0.1 L/min. It is obvious that the conversion rate values are lower than those at 4.5 mm due to the lower residence time and ammonia reaction time at a gap distance of 1 mm.

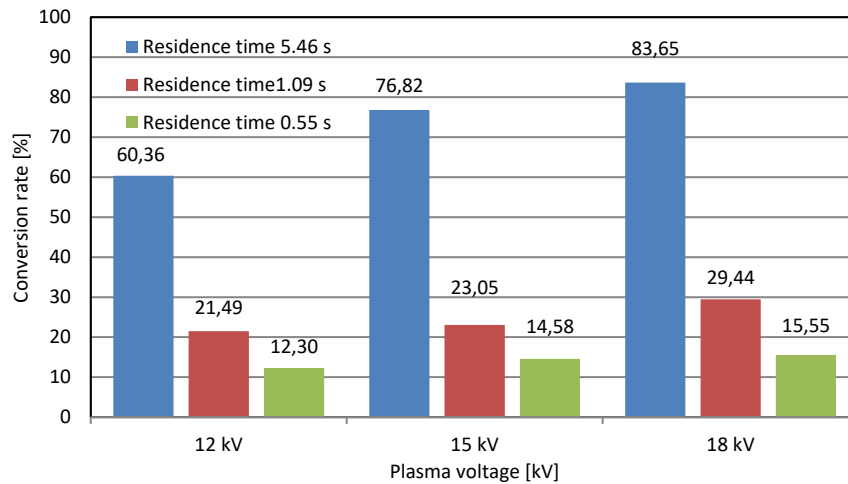


Figure 6. NH_3 conversion rate vs. residence time in PPR with electrode gap of 4.5 mm

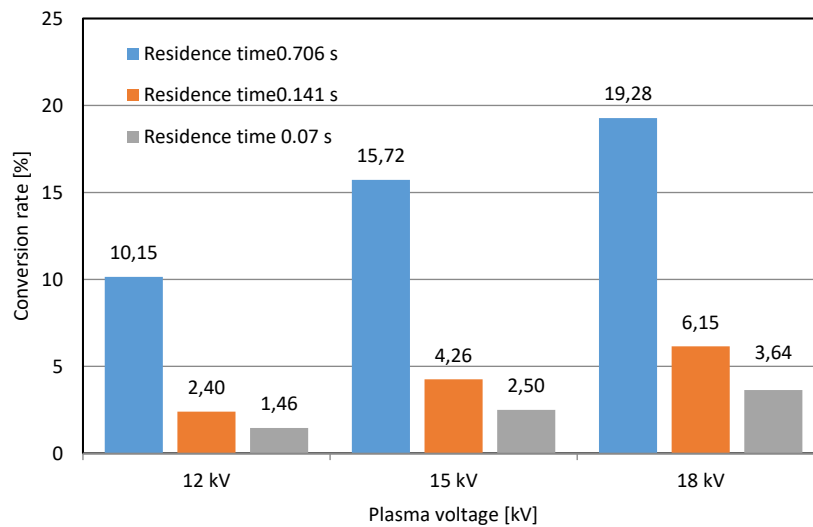


Figure 7. NH_3 conversion rate vs. residence time in PPR with electrode gap of 1 mm

Heat transfer distribution analysis

Figure 8 compares the heat transfer distribution across the dielectric, metal electrodes, and heat loss to the atmosphere at 12 kV. These results were determined based on the energy distribution equations discussed in the previous section. 80% of the DBD plasma input power was transferred as heat to both electrodes [26], around 65% was transferred to the dielectric electrode, and 15% was transferred to the metal or ground electrode. This is due to the micro discharge concentration spreading on the dielectric glass electrode's surface in a much larger area than the filament diameter.

Figure 9 shows the heat transfer distribution to the dielectric electrode at different voltages and NH₃ input flow rates. The heat transfer distribution at 12 kV was higher than at 15 kV and 18 kV. The variation of the heat transfer distribution of the dielectric electrodes was slightly decreased at low ammonia flow rate, and the amount is related to the enthalpy gained by the ammonia feed gas. Secondary electron emissions deliver more ionization, which leads to higher metal electrode heating than that of the dielectric electrode.

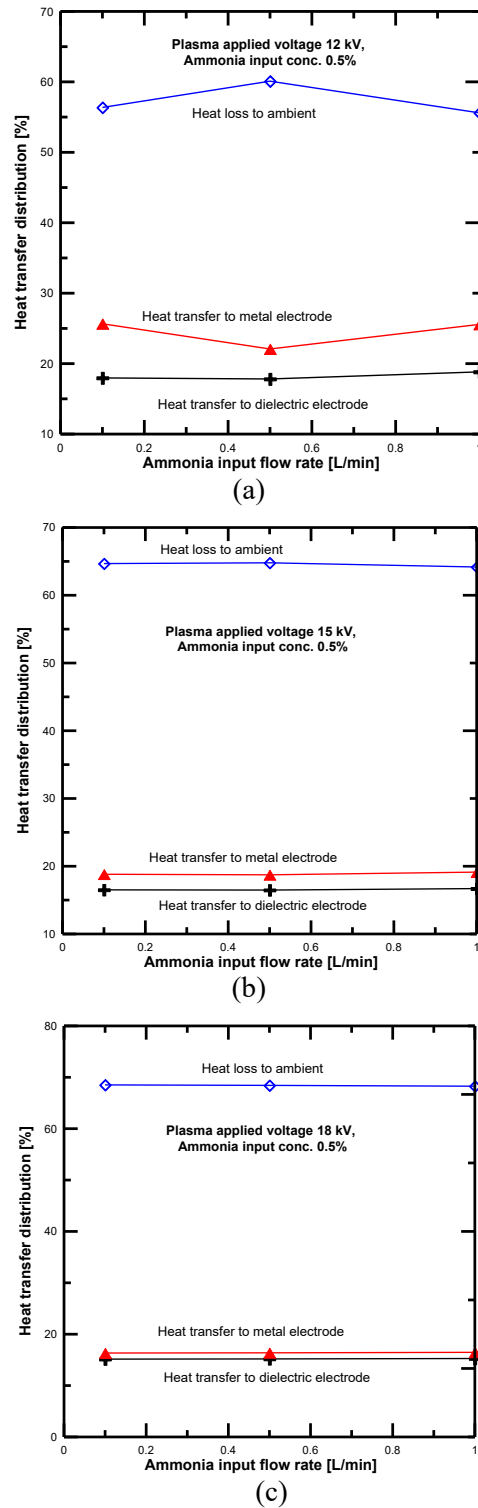


Figure 8. Heat transfer distribution in PPR with electrode gap distance of 4.5 mm: plasma voltage 12 kV (a); plasma voltage 15 kV (b) and plasma voltage 18 kV (c)

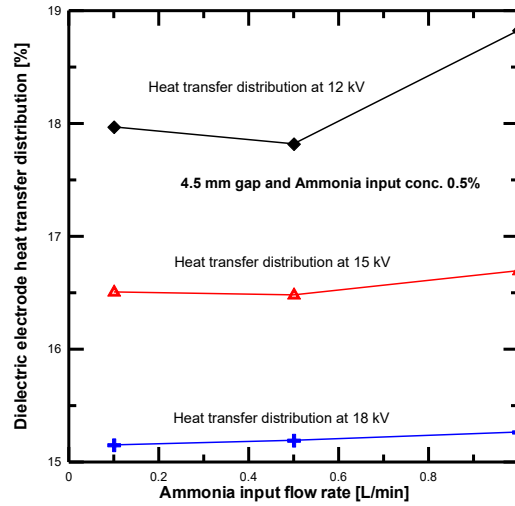


Figure 9. Dielectric electrode heat transfer distribution

Figure 10 compares the heat transfer distribution of the metal electrode at different voltages. The heat transfer distribution increased with ammonia input flow rate at 15 and 18 kV. The heat transfer distribution was clearly decreased at an NH_3 flow rate of 0.5 L/min and 12 kV. It has been reported that the heat transfer mechanism is not affected by the feed gas' physical properties but is influenced by changes in the plasma structure [21].

Additionally, the heat transfer distribution of the metal electrode was higher than that obtained from the dielectric electrode. The total heat transfer rate at different input flow rates and voltages is shown in **Figure 11**. It is clear from this figure that the total heat transfer rate at 18 kV was much higher than at 15 kV and 18 kV. Most of the plasma heat was transferred to the high-voltage electrode direction due to the concentration of micro discharges at the electrode surface. Furthermore, the DBD plasma heat transfer mechanism was not affected by the changes of the feed gas' physical properties, while the ammonia's decomposition behavior using DBD plasma was obviously changed.

Figure 12 presents the overall heat transfer coefficient at different input flow rates and plasma voltages. It is clear that the overall heat transfer coefficient increased with the voltage. Furthermore, the overall heat transfer coefficient at the ammonia flow rate of 1 L/min was higher than at 0.5 and 0.1 L/min. Conversely, the overall heat transfer coefficient at the high ammonia flow rate exceeded those of the lower ones, while the conversion rate results at the same ammonia flow rate were lower.

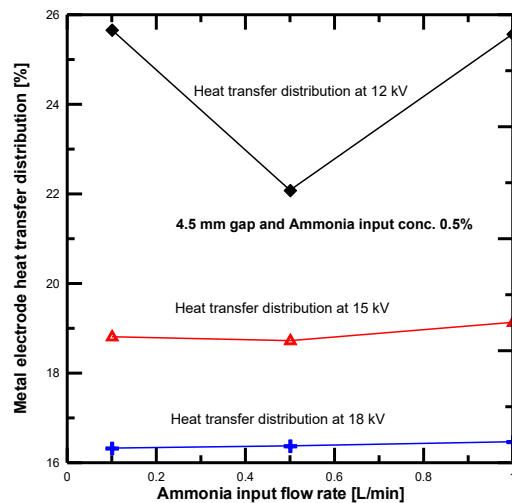


Figure 10. Metal electrode heat transfer distribution

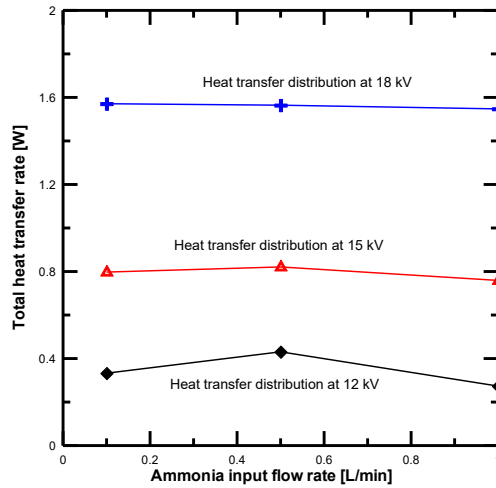


Figure 11. Total heat transfer rate distribution at different plasma voltages

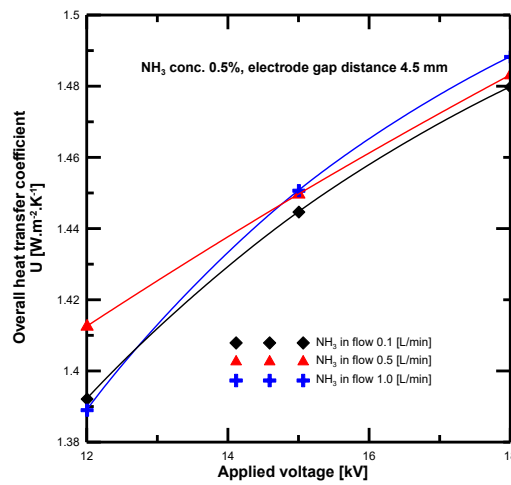


Figure 12. Overall heat transfer coefficient at different NH₃ flow rates

Figure 13 compares the energy efficiency of both reactors with different electrode gap distances and electric power. It is clear that the energy efficiency was higher at a gap distance of 4.5 mm than at 1 mm. The maximum energy efficiencies at 4.5 mm with input flow rates of 1, 0.5, and 0.1 L/min were 0.1936%, 0.178%, and 0.1057%, respectively. The maximum energy efficiencies at 1 mm with ammonia input flow rates of 1, 0.5, and 0.1 L/min were 0.0428%, 0.038% and 0.022%, respectively.

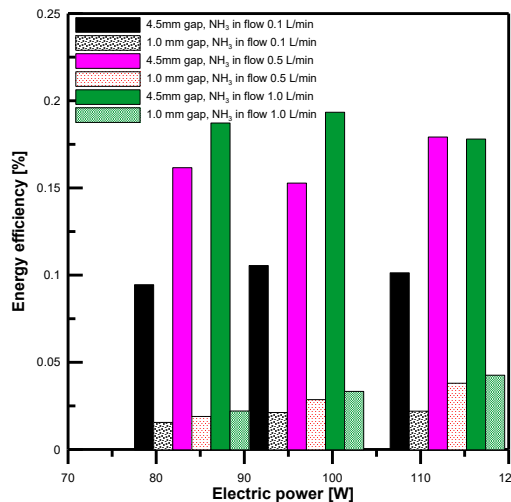


Figure 13. Comparison of energy efficiency versus input electric power

CONCLUSIONS

In this study, ammonia-argon base gas was decomposed into hydrogen and nitrogen gas by atmospheric-pressure DBD plasma. Ammonia gas was fed into PPRs with electrode gap distances of 1 mm and 4.5 mm. The hydrogen production was affected by the electrode gap distance. The hydrogen concentration and flow rate at a gap distance of 4.5 mm results were much higher than at 1 mm.

The effect of the residence time on the hydrogen conversion was also investigated. The maximum conversion rates at 4.5 mm and 1 mm were 83% and 19.29%, respectively. The heat transfer distribution of metal, dielectric electrodes, and heat loss to the atmosphere were determined at different voltages, and most of the heat generation was transferred to the dielectric electrode surface due to the concentration of micro discharges near the high-voltage electrode. The heat transfer mechanism was not affected by the ammonia physical properties, while the ammonia decomposition by the DBD plasma was obviously changed.

The energy efficiency of NH₃ decomposition was determined at different input power. The maximum obtained energy efficiencies with an NH₃ concentration of 5% and gap distance of 4.5 mm were 0.1936%, 0.178%, and 0.1057% at ammonia input flow rates of 1, 0.5, and 0.1 L/min, respectively. Those at a gap distance of 1 mm were 0.0428%, 0.038%, and 0.022%, respectively.

ACKNOWLEDGMENT

The authors would like to thank *Prof. Shinji Kambara* (Environmental and energy systems department-Gifu University-Japan) for his continuous support.

REFERENCES

1. Schüth, F., Palkovits, R., Schlögl, R. and Su, D. S., Ammonia as a Possible Element in an Energy Infrastructure: Catalysts for Ammonia Decomposition, *Energy Environ. Sci.*, Vol. 5, No. 4, pp 6278-6289, 2012, <https://doi.org/10.1039/C2EE02865D>
2. Satyapal, S., Petrovic, J., Read, C., Thomas, G. and Ordaz, G., The U.S. Department of Energy's National Hydrogen Storage Project: Progress Towards Meeting Hydrogen-Powered Vehicle Requirements, *Catal. Today*, Vol. 120, No. 3-4, pp 246-256, 2007, <https://doi.org/10.1016/j.cattod.2006.09.022>
3. El-Shafie, M., Kambara, S. and Hayakawa, Y., Hydrogen Production Technologies Overview, *J. Power and En. Eng.*, Vol. 7, No. 1, pp 107-154, 2019, <https://doi.org/10.4236/jpee.2019.71007>
4. Bassani, A., Previtali, D., Pirola, C., Bozzano, G., Colombo, S. and Manenti, F., Mitigating Carbon Dioxide Impact of Industrial Steam Methane Reformers by Acid Gas to Syngas Technology: Technical and Environmental Feasibility, *J. Sustain. Dev. Energy Water Environ. Syst.*, Vol. 8, No. 1, pp 71-87, 2020, <https://doi.org/10.13044/j.sdewes.d7.0258>
5. dos Anjos, M. M., Tenenwurcel, D. R., Santos, L. A. O., Ferreira, W. R., Costa, A. L. and Pereira, E. M. D., Low Carbon Transition Through Renewables Sources – An Overview of the Renewable Energy Program in the State of Minas Gerais, *J. Sustain. Dev. Energy Water Environ. Syst.*, Vol. 8, No. 2, pp 252-267, 2020, <https://doi.org/10.13044/j.sdewes.d7.0295>
6. Sadooghi, P. and Rauch, R., Experimental and Modeling Study of Hydrogen Production from Catalytic Steam Reforming of Methane Mixture with Hydrogen Sulfide, *Int. J. Hydrogen Energy*, Vol. 40, No. 33, pp 10418-10426, 2015, <https://doi.org/10.1016/j.ijhydene.2015.06.143>
7. Kim, N. Y., Yang, E.-H., Lim, S.-S., Jung, J. S., Lee, J.-S., Hong, G. H., Noh, Y. S., Lee, K. Y. and Moon, D. J., Hydrogen Production by Steam Reforming of Methane Over Mixed Ni/MgAl+CrFe₃O₄ Catalysts, *Int. J. Hydrogen Energy*, Vol. 40, No. 35, pp 11848-11854, 2015, <https://doi.org/10.1016/j.ijhydene.2015.06.104>
8. Mikulandrić, R., Böhning, D. and Lončar, D., Modelling of Temperature and Syngas Composition in a Fixed Bed Biomass Gasifier using Nonlinear Autoregressive Networks,

- J. Sustain. Dev. Energy Water Environ. Syst.*, Vol. 8, No. 1, pp 145-161, 2020, <https://doi.org/10.13044/j.sdewes/d7.0263>
9. Saleem, F., Zhang, K. and Harvey, A. P., Decomposition of Benzene as a Tar Analogue in CO₂ and H₂ Carrier Gases, Using a Non-Thermal Plasma, *Chem. Eng. J.*, Vol. 360, pp 714-720, 2019, <https://doi.org/10.1016/j.cej.2018.11.195>
 10. Burlica, R., Shih, K. Y. and Locke, B., Formation of H₂ and H₂O₂ in a Water-Spray Gliding Arc Nonthermal Plasma Reactor, *Ind. Eng. Chem. Res.*, Vol. 49, No. 14, pp 6342-6349, 2010, <https://doi.org/10.1021/ie100038g>
 11. El-Shafie, M., Kambara, S., Hayakawa, Y. and Mura, T., Preliminary Results of Hydrogen Production from Water Vapor Decomposition Using DBD Plasma in a PMCR Reactor, *Int. J. Hydrogen Energy*, Vol. 44, No. 36, pp 20239-20248, 2019, <https://doi.org/10.1016/j.ijhydene.2019.05.199>
 12. Rehman, F., Lozano-Parada, J. H. and Zimmerman, W. B., A Kinetic Model for H₂ Production by Plasmolysis of Water Vapors at Atmospheric Pressure in a Dielectric Barrier Discharge Micro-Channel Reactor, *Int. J. Hydrogen Energy*, Vol. 37, No. 23, pp 17678-17690, 2012, <https://doi.org/10.1016/j.ijhydene.2012.08.113>
 13. Kogelschatz, U., Filamentary, patterned and diffuse barrier discharges. *IEEE Transactions on Plasma Science*, 30(4), 1400–1408. [10.1109/TPS.2002.804201](https://doi.org/10.1109/TPS.2002.804201)
 14. Borcia, G., Anderson, C. A. and Brown, N. M. D., Dielectric Barrier Discharge for Surface Treatment: Application to Selected Polymers in Film and Fibre Form, *Plasma Sources Sci. Technol.*, Vol. 12, No. 3, pp 335-344, 2003, <https://doi.org/10.1088/0963-0252/12/3/306>
 15. Okazaki, K. and Nozaki, T., Ultrashort Pulsed Barrier Discharges and Applications, *Pure Appl. Chem.*, Vol. 74, No. 3, pp 447-452, 2002, <https://doi.org/10.1351/pac200274030447>
 16. Van Durme, J., Dewulf, J., Leys, C. and Van Langenhove, H., Combining non-thermal plasma with heterogeneous catalysis in waste gas treatment: A review, *Appl. Catal. B- Environ.*, 2008, Vol. 78, 324-333. <https://doi.org/10.1016/j.apcatb.2007.09.035>
 17. Iza, F., Kim, G. J., Lee, S. M., Lee, J. K., Walsh, J. L., Zhang, Y. T. and Kong, M. G., Microplasmas: Sources, Particle Kinetics, and Biomedical Applications, *Plasma Proc. and Polym.*, Vol. 5, 322, 2008. <https://doi.org/10.1002/ppap.200700162>
 18. Borcia, G., Anderson, C. A. and Brown, N. M. D., Dielectric barrier discharge for surface treatment: application to selected polymers in film and fibre form, *Plasma Sources Sci. Technol.*, Vol. 12, 335, 2003. <https://doi.org/10.1088/0963-0252/12/3/306>
 19. Corke, T. C., Enloe, C. L. and Wilkinson, S. P., Dielectric Barrier Discharge Plasma Actuators for Flow Control, *Annu. Rev. Fluid Mech.*, Vol. 42, 505, 2010. <https://doi.org/10.1146/annurev-fluid-121108-145550>
 20. Eliasson, B., Hirth, M. and Kogelschatz, U., Ozone synthesis from oxygen in dielectric barrier discharges, *J. Phys. D: Appl. Phys.*, Vol. 20, pp 1421-1427, 1987. <https://doi.org/10.1088/0022-3727/20/11/010>
 21. Nozaki, T., Miyazaki, Y., Unno, Y. and Okazaki, K., Energy Distribution and Heat Transfer Mechanisms in Atmospheric Pressure Non-Equilibrium Plasmas, *J. Phys. D: Appl. Phys.*, Vol. 34, No. 23, pp 3383-3390, 2001.
 22. El-Shafie, M., Kambara, S. and Hayakawa, Y., Study of the Reactor Temperature Effect on H₂ Production from Steam Decomposition Using DBD Plasma, *Energy Reports*, Vol. 6, Supp. 2, pp 45-51, 2020, <https://doi.org/10.1016/j.egyr.2019.11.040>
 23. Massines, F., Rabehi, A., Decomps, P., Gadri, R. B., Segur, P. and Mayoux, C., Experimental and theoretical study of a glow discharge at atmospheric pressure controlled by dielectric barrier, *J. Appl. Phys.*, Vol. 83, No. 6, pp 2950-2957, 1998. <https://doi.org/10.1063/1.367051>
 24. Li, S., Gu, F., Tang, B., Ma, T. and Wang, X., Numerical Analysis of the Momentum and Heat Transfer in an Atmospheric Pressure Dielectric Barrier Discharge, *AIP Advances*, Vol. 9, No. 3, 035219, 2019, <https://doi.org/10.1063/1.5086791>

25. Incropera, F. P., Dewitt, D. P., Bergman, T. L. and Lavine, A. S., *Introduction to Heat Transfer (5th ed.)*, John Wiley & Sons Inc., New Jersey, USA, 2007.
26. Churchill, S. W. and Chu, H. H. S., Correlating Equations for Laminar and Turbulent Free Convection from a Vertical Plate, *Int. J. Heat and Mass Trans.*, Vol. 18, No. 11, pp 1323-1329, 1975, [https://doi.org/10.1016/0017-9310\(75\)90243-4](https://doi.org/10.1016/0017-9310(75)90243-4)



Paper submitted: 30.03.2020
Paper revised: 12.07.2020
Paper accepted: 12.07.2020